

Mid-Pleistocene climate transition triggered by Antarctic ice-sheet growth

An Zhisheng^{1,2,3,4*}, Weijian Zhou^{1,2,3,5}, Zeke Zhang^{1,2,4}, Xu Zhang^{6,7*}, Zhonghui Liu^{1,8*},
Youbin Sun^{1,2,5}, Steven C. Clemens⁹, Lixin Wu^{5,10}, Jiaju Zhao^{1,2}, Zhengguo Shi^{1,2,5}, Xiaolin
Ma^{1,5}, Hong Yan^{1,2,5}, Gaojun Li⁴, Yanjun Cai², Jimin Yu^{5,11}, Yuchen Sun¹², Siqi Li⁶, Yu'ao
Zhang⁶, Christian Stepanek¹², Gerrit Lohmann¹², Guocheng Dong¹, Hai Cheng², Yu Liu¹,
Zhangdong Jin^{1,2}, Tao Li¹³, Yifei Hao¹, Jing Lei^{1,14}, Wenju Cai^{5,10,15}

Affiliations:

¹State Key Laboratory of Loess and Quaternary Geology, Institute of Earth Environment, Chinese Academy of Sciences, Xi'an 710061, China.

²Institute of Global Environmental Change, Xi'an Jiaotong University, Xi'an 710049, China.

³Interdisciplinary Research Center of Earth Science Frontier, Beijing Normal University, Beijing 100875, China.

⁴Department of Earth and Planetary Sciences, Nanjing University, Nanjing 210023, China.

⁵Laoshan Laboratory, Qingdao, 266000, China

⁶State Key Laboratory of Tibetan Plateau Earth System, Resources and Environment (TPESRE), Institute of Tibetan Plateau Research, Chinese Academy of Sciences, Beijing 100101, China.

⁷British Antarctic Survey, Cambridge CB3 0ET, UK

⁸Department of Earth Sciences, The University of Hong Kong, Hong Kong, China.

⁹Department of Earth, Environmental and Planetary Sciences, Brown University, Providence, RI 02912, USA.

¹⁰Key Laboratory of Physical Oceanography/Institute for Advanced Ocean Studies, Ocean University of China, Qingdao 266100, China.

¹¹Research School of Earth Sciences, Australian National University, Canberra, ACT 2601, Australia.

¹²Alfred Wegener Institute Helmholtz Center for Polar and Marine Research, Bremerhaven 27570, Germany.

¹³Key Laboratory of Palaeobiology and Petroleum Stratigraphy, Nanjing Institute of Geology and Palaeontology, Chinese Academy of Sciences, Nanjing 210008, China

¹⁴Xi'an Institute for Innovative Earth Environment Research, Xi'an 710061, China.

¹⁵Centre for Southern Hemisphere Oceans Research (CSHOR), CSIRO Oceans and Atmosphere, Hobart 7004, Australia.

*Corresponding author. Email: anzs@loess.llqg.ac.cn (A. Z. S.); xu.zhang@itpcas.ac.cn (X. Z.); zhliu@hku.hk (Z. L.)

Abstract:

Despite extensive investigation, the nature and causes of the Mid-Pleistocene Transition remain enigmatic. Here we assess its linkage to asynchronous development of bi-polar ice sheets by synthesizing Pleistocene mid- to high-latitude proxy records linked to hemispheric ice sheet evolution. Our results indicate substantial growth of the Antarctic Ice Sheets at 2.0–1.25 Ma, preceding the rapid expansion of Northern Hemisphere ice sheets after ~1.25 Ma. Proxy-model comparisons suggest that Antarctic ice sheet and associated Southern Ocean sea-ice expansion can induce northern high-latitude cooling and enhanced moisture transport to the Northern Hemisphere, thus triggering the mid-Pleistocene climate transition. The dynamical processes involved are crucial for assessing modern global warming that is already inducing asynchronous bi-polar melting of ice sheets.

One-Sentence Summary: Early Antarctic ice sheet and associated Southern Ocean sea-ice expansion triggered the mid-Pleistocene climate transition.

Main Text:

The formation and evolution of bi-polar ice sheets not only played critical roles in driving global climatic changes during the Cenozoic but are also important for projecting future climate change. Cenozoic global climate has been characterized by asynchronous development of ice sheets, from the unipolar glaciation of Antarctica to bi-polar glaciation (1). The Antarctic Ice Sheets (AIS) predominated during the early Oligocene to late Pliocene, after which the Northern Hemisphere Ice Sheets (NHIS) evolved, ultimately driving large-amplitude glacial-interglacial fluctuations of the Pleistocene (1, 2). The Mid-Pleistocene Transition (MPT) is characterized by a shift from symmetrical 41-kyr climatic cycles before ~1.25 Ma to asymmetrical ~100-kyr cycles afterwards (2, 3). In the absence of any appreciable trends in astronomical forcing over this period, the origin of the ~100-kyr ice age cycles is largely attributed to feedbacks and internal changes in the Earth's climate system. Proposed mechanisms include Northern Hemisphere (NH) bedrock and regolith erosion beneath the ice sheets (3), gradual atmospheric CO₂ decline (4), AIS expansion from terrestrial to marine margin-based ice sheets (5), and deep ocean circulation reorganization (6). These hypotheses cover most of the possible internal and external factors and have significantly improved our understanding of the MPT. However, asynchronous development of bi-polar ice sheets has not yet been explored as a potential driver as there is currently no direct evidence to differentiate hemispheric contributions to ice-sheet growth from the geologic record. Here we integrate Pleistocene climate records closely associated with hemispheric ice-sheet evolution, and reconstruct hemispheric ice volume changes using mid-latitude sea surface temperature (SST) records. Supported by model simulations, we propose that from ~2 to 1.25 Ma AIS growth and associated climate feedbacks altered cross-equatorial meridional transport of heat and moisture to the NH, promoting the MPT.

Synthesized Pleistocene climate records

We use mid-latitude SSTs to perform a semi-quantitative reconstruction of hemispheric ice volume changes (Materials and Methods). Ice rafted debris (IRD), dust iron flux, cosmogenic-nuclide exposure ages, and grain size-based reconstructions of the westerlies are also integrated to reflect Pleistocene hemispheric ice-sheet development and its impacts (fig. S1, Fig. 1). Southern Ocean SST, Antarctic air temperature, and modeled AIS changes are strongly coupled (7, 8). Expansion of the terrestrial cryosphere, increasing surface albedo, sea-ice expansion and increasing dust flux, drive ~65% of global SST decline and substantial high-latitude SST cooling (by >8°C) during glacial stages (9). Hence, mid- to high-latitude (>40°N/S) SST sensitively responds to ice-sheet changes (10) and thus can be used to reconstruct hemispheric ice sheet evolution.

We utilize alkenone-based SST records from mid-latitude oceans to generate Pleistocene SST reconstructions separately for each hemisphere. These are verified by shorter stacks over the last 500 kyr that are based on more available SST records (Materials and Methods, Supplementary Text, fig. S2, table S1). The two Pleistocene stacks are interpreted as reliable indicators of hemispheric ice-sheet development (Fig. 1B, 1H). The Southern Hemisphere (SH) SST stack indicates a long-term cooling from ~2.0 to 1.25 Ma (Fig. 1B), indicative of AIS growth. This is substantiated by decreased IRD from ~2.0–1.6 Ma to 1.6–1.25 Ma at ODP 1101 in the Antarctic polar region (11) (Fig. 1C, fig. S3), reflecting reduced presence of “dirty” icebergs and thus increased marine-based AIS and extended sea ice from ~2.0 Ma onwards (12–14). In the subpolar region, IRD showed amplification from the beginning of the record (~1.65 Ma) and increased substantially at ~1.25 Ma (15) (Fig. 1C, fig. S3), indicating further sea-ice expansion from high- to mid-latitude ocean around the MPT. Dust iron flux to the South Atlantic also increased greatly

during glacial stages at 1.6–1.25 Ma (16) (Fig. 1D, fig. S3E). Off west Australia, the trend of precipitation (as evidenced by a Ti/Ca record) indicates enhanced continental aridification at 2.0–1.25 Ma (17) (Fig. 1E). Finally, at Roberts Massif, East AIS, cosmogenic-nuclide exposure-ages show high frequency of occurrences at 1.7–1.0 Ma (18) (Fig. 1F), corroborated by thick ice sheets and enhanced glacial activity found in other Antarctic regions (Supplementary Text). These multiple, independent lines of evidence indicate substantial AIS growth, sea-ice expansion, and associated impacts from 2.0 to 1.25 Ma, which is at a time well before the MPT.

By contrast, the NH SST stack shows remarkable glacial cooling during ~1.25–0.7 Ma (Fig. 1H), indicative of the delayed NHIS growth compared to the AIS. In the North Atlantic, IRD events deduced from a bulk carbonate $\delta^{18}\text{O}$ record from IODP U1308 started to increase at ~1.3 Ma (19) (Fig. 1I). Dust deposition (20) amplified substantially after ~1.3 Ma (Fig. 1J, fig. S4). Inorganic carbon isotopes ($\delta^{13}\text{C}$) from inland Asia (Lop Nur; Fig. 1L) and loess grain size from the Kunlun Mountains show continued continental aridification and enhanced westerlies circulation at 1.25–0.7 Ma (21, 22), both linked to the NHIS growth during the MPT. As winter monsoon intensity is strongly associated with the NHIS through the Siberian High (23), the thick, coarse loess layer (L₁₅LL₁) at the classic Luochuan profile on the Chinese Loess Plateau is regarded as a marker layer for the MPT initiation on land (Supplementary Text, fig. S5, C–G). Coarsened mean grain size in loess layers (Fig. 1K) suggests an expanded glacial NHIS since ~1.25 Ma (24). Combined, these multiple NH and SH proxies reveal substantial AIS growth at 2.0–1.25 Ma, preceding the rapid growth of the NHIS after ~1.25 Ma (Fig. 1). At ~1.25 Ma, wavelet spectra of the benthic marine $\delta^{18}\text{O}$ stack, of NH and SH SST stacks, of loess grain size, and of Southern Ocean iron flux all indicate the shift of dominant periodicity from 41 kyr to ~100 kyr (fig. S5A).

Reconstructed bi-polar ice sheets

Utilizing our SST stacks and existing ice-sheet records, we established a transfer function between SST and ice volume separately for each hemisphere (Materials and Methods, fig. S6, table S2). A recent stack of extratropical SST for the two hemispheres (25) shares great similarity with our hemispheric SST stacks. Both extratropical and our hemispheric SST stacks indicate that cooling of the SH prior to the MPT preceded that of the NH (fig. S7), thus substantiating the critical feature of asynchronous hemispheric cooling reported here. The sum of reconstructed hemispheric ice volume shows strong consistency with both the global ice volume derived from the benthic $\delta^{18}\text{O}$ stack (2) and model simulations (26) ($R^2 = 0.62, 0.60$) (Fig. 2C). In general, our estimated global ice volume is slightly lower before ~1.25 Ma than the latter two (Fig. 2C). The transformed SST stacks are thus interpreted as reflecting independent evolution of the NH and SH ice sheets (Fig. 2, fig. S8B, S8D). Consideration of chronology uncertainty (± 0.5 kyr and ± 2.5 kyr) in the SST stacks (Materials and Methods) does not impact the overall structure of estimated global and hemispheric ice volume (fig. S8, S9). However, applying a larger age uncertainty (± 2.5 kyr) could reduce the estimates of glacial ice volume before ~1.25 Ma unproportionally (fig. S9), also noted in the recent SST stacking (25).

Our reconstruction of hemispheric ice volume, strongly supported by the multiple lines of independent evidence presented above (Fig. 1), indicates that SH glacial ice volume started to increase from ~2.0 Ma. The estimated AIS increase at 2.0–1.25 Ma is ~9 m in equivalent sea level (ESL) (Fig. 2A). By contrast, NH glacial ice volume did not change appreciably before the MPT and started to increase around 1.25 Ma. At 1.25–0.7 Ma, the NH glacial ice volume increased by ~43 m ESL, and afterwards remained at a high level (95 ± 27 m) (Fig. 2A). Reconstructed SH glacial ice volume was predominant before ~1.25 Ma, while NH glacial ice volume gradually

became dominant thereafter (Fig. 2B). Furthermore, from ~1.25 Ma onwards, both NHIS and AIS varied in concert for most glacial periods (fig. S8E), perhaps related to the transformation from terrestrial to marine margin-based AIS at the time (5). Although marine-based AIS was proposed to have developed during 3–2 Ma, inferred from a recent reconstruction with greater ice volume change at the time (27) (Materials and Methods), the dynamical AIS prior to the MPT, as indicated by presence of “dirty” icebergs (12–14), would suggest a limited extent of marine ice-shelves.

Mechanism for MPT initiation

Since orbital parameters (Fig. 3A, 3B) are unlikely to be the direct driver for the MPT initiation (3), long-term atmospheric CO₂ decline has been considered as one of the main drivers (4). However, a compilation of Pleistocene CO₂ records reveals a decrease in CO₂ concentration at ~2.3–2.0 Ma, followed by a relatively stable level at ~2.0–0.9 Ma and a decline thereafter (Fig. 3C, Supplementary Text). Hence, although low CO₂ could have promoted ice-sheet growth (4), available CO₂ data, limited by data resolution and proxy uncertainty, do not provide sufficient evidence for this direct dynamical link to the MPT initiation.

Here we hypothesize that long-term AIS growth and its associated feedbacks are a potentially important precursor to, or even a direct trigger of, the MPT. That is, AIS growth before the MPT (Fig. 3D) and the associated sea-ice expansion from southern high latitudes toward mid-latitudes (Figs. 1C, 3E, 3F, fig. S10B) might have reduced global temperature and altered atmosphere/ocean circulation, inducing temperature and moisture conditions favorable for the NHIS growth (Fig. 3J) and hence the MPT initiation. AIS growth during the early to mid-Pleistocene can be decomposed in contributions of area expansion and elevation increase (e.g., (5, 28)). To evaluate their individual and synergistic impacts on global climate, we apply the fully coupled ocean – atmosphere – land-surface and vegetation model COSMOS (Materials and Methods, Fig. 4, figs. S11, S12, table S3). In our sensitivity experiments we consider AIS area, AIS height and a superposition of AIS area and height under both interglacial and glacial atmospheric CO₂ levels (280 ppm and 220 ppm from “Blue Ice” (29), Fig. 3C). Intercomparison amongst all the AIS experiments shows that those including AIS area expansion are more consistent with multiple proxy records (Fig. 3E, 3F, 3I, fig. S10), which are characterized by sea-ice expansion in both Southern Ocean and northern high latitudes (Fig. 4A, 4E, fig. S12) and weakened Atlantic Meridional Overturning Circulation (AMOC) (Fig. 4D, 4H). Furthermore, the substantial temperature decrease in NHIS nucleation regions is in line with the ice-albedo feedback on the global energy balance and the weakened AMOC (Fig. 4B, 4F). Of particular importance is that these responses were strengthened substantially as atmospheric CO₂ decreased from 280 to 220 ppm (Fig. 4), indicating the existence of internal feedbacks amplifying the impacts of AIS growth on NHIS development.

Southern Ocean sea-ice variability on sub-orbital, orbital, and longer timescales is coupled with AIS growth (15, 30, 31). Sea-ice cover is, *per se*, sensitive to changes in regional temperature and wind fields that are themselves controlled by the AIS (15, 32) and by atmospheric CO₂ levels (33). Formation and export of Southern Ocean sea ice are of crucial importance for dense Antarctic Bottom Water formation and hence for the development of stratified glacial deep oceans and associated carbon sequestration during glaciations (34–37). Together with findings from proxy records, we suggest that the AIS-induced equatorward expansion of sea-ice cover in the Southern Ocean (Figs. 1C, 3E, 3F) is the key to linking long-term AIS growth to NHIS development. To confirm this, we further conducted three Southern Ocean sea-ice sensitivity experiments by expanding the Southern Ocean sea-ice margin equatorward by ~3° under the mid-Pliocene (38), pre-industrial and Last Glacial Maximum (36) boundary conditions, respectively (Materials and

Methods, [table S3](#)). The results are consistent with the climatic impacts caused by the AIS expansion ([Fig. 4](#)), and also show amplified cooling amplitudes under the relatively cold climate of the Last Glacial Maximum ([fig. S13](#)). Overall, our model results suggest that long-term AIS growth and associated climate feedbacks (e.g., sea-ice expansion, [fig. S13](#)) from ~2.0 to 1.25 Ma would induce global cooling, creating the colder preconditions favorable for NHIS growth during glacial stages ([Fig. 4](#)), and setting the stage for amplified NHIS ice volume thereafter.

Sea-ice expansion surrounding Antarctica would cool the Southern Ocean with an effect to increase meridional pressure gradients in the SH. This would result in an equatorward shift of austral westerlies and Hadley circulation, and enhanced cross-equatorial flow (39-43). At 2.0–1.25 Ma, substantial strengthening of the Asian summer monsoon, indicated by our new loess microcodium $\delta^{18}\text{O}$ record ([Fig. 3H](#), [fig. S14](#), Materials and Methods, Supplementary Text), is likely linked to the cross-equatorial pressure gradient changes that are caused by the NH-SH SST gradient ([Fig. 3G](#)) and supported by modeling results ([Fig. 4C](#), [4G](#), [fig. S13](#)). Hence, southern high-latitude cooling can drive a northward migration of the Intertropical Convergence Zone (39), leading to a relative increase in moisture content in the NH as compared to the SH ([fig. S13](#)). This effect, aided by the enhanced storm activity caused by the strengthened low- to high-latitude temperature gradient (44) ([Fig. 4](#)), might have promoted northward moisture transport from the North Pacific and the North Atlantic to NHIS nucleation regions. As cold conditions tend to suppress atmospheric moisture content ([fig. S13](#)), the impacts of moisture transport may have been more effective during glacial inception but diminished towards the coldest glacial maxima.

In summary, our reconstructions show the asynchronous evolution of Pleistocene hemispheric ice sheets characterized by substantial AIS growth from ~2.0 to 1.25 Ma, while rapid NHIS growth only commenced thereafter. We postulate that the MPT initiation was triggered by AIS expansion, when its cumulative effects reached a critical threshold at ~1.25 Ma. Our results suggest that AIS and associated sea-ice expansion changed atmospheric and oceanic circulation, inducing global cooling and increased moisture transport to northern high latitudes, which likely promoted NHIS growth at ~1.25 Ma, an important time marker for the MPT onset; the relatively low eccentricity at ~1.25 Ma also provided a favorable condition for the accumulation of continental ice sheets. Together with the transformation from terrestrial to marine margin-based AIS, substantial ice-sheet growth in the two hemispheres would have been sustained at the relatively low summer insolation maximum and provided a prerequisite for the occurrence of ~100-kyr ice age cycles (5). Our proxy-model comparison suggests that asynchronous development of hemispheric ice sheets is indispensable for understanding global climate change. Accordingly, with the accelerated, asynchronous melting of modern bi-polar ice sheets, enhanced perturbations within the climate system could be anticipated in the near future. These effects warrant consideration towards improving climate projections and our understanding of regional to global impacts of anthropogenic climate change.

References and Notes

1. T. Westerhold *et al.*, *Science* **369**, 1383 (2020).
2. L. E. Lisiecki, M. E. Raymo, *Paleoceanography* **20**, 1-16 (2005).
3. P. U. Clark *et al.*, *Quaternary Science Reviews* **25**, 3150-3184 (2006).
4. M. Willeit, A. Ganopolski, R. Calov, V. Brovkin, *Science Advances* **5**, eaav7337 (2019).
5. M. E. Raymo, L. E. Lisiecki, K. H. Nisancioglu, *Science* **313**, 492-495 (2006).

6. E. Tziperman, H. Gildor, *Paleoceanography* **18**, 1-1-1-8 (2003).
7. D. Pollard, R. M. Deconto, *Nature* **458**, 329-332 (2009).
8. R. Uemura *et al.*, *Nature Communications* **9**, 961 (2018).
9. J. E. Tierney *et al.*, *Nature* **584**, 569-573 (2020).
- 5 10. E. J. Rohling, M. Medina-Elizalde, J. G. Shepherd, M. Siddall, J. D. Stanford, *Journal of Climate* **25**, 1635-1656 (2012).
11. E. A. Cowan, in *Ocean Drilling Program, Proceedings*, P. F. Barker, Camerlenghi, A., Acton, G.D., Ramsay, A.T.S, Ed. (Scientific Results, 2001), vol. 178, pp. 1-22.
12. M. E. Weber *et al.*, *Nature* **510**, 134-138 (2014).
- 10 13. I. Bailey *et al.*, *Paleoceanography and Paleoclimatology* **37**, e2022PA004433 (2022).
14. T. Naish *et al.*, *Nature* **458**, 322-328 (2009).
15. A. Starr *et al.*, *Nature* **589**, 236-241 (2021).
16. A. Martínez-García *et al.*, *Nature* **476**, 312 (2011).
17. B. Petrick *et al.*, *Scientific Reports* **9**, 13 (2019).
- 15 18. A. Balter-Kennedy, G. Bromley, G. Balco, H. Thomas, M. S. Jackson, *The Cryosphere* **14**, 2647-2672 (2020).
19. D. A. Hodell, J. E. T. Channell, *Climate of the Past* **12**, 1805-1828 (2016).
20. B. D. A. Naafs *et al.*, *Earth and Planetary Science Letters* **317-318**, 8-19 (2012).
21. W. Liu *et al.*, *Geology* **48**, 782-786 (2020).
- 20 22. X. Fang *et al.*, *Proceedings of the National Academy of Sciences* **117**, 24729 (2020).
23. Q. Hao *et al.*, *Nature* **490**, 393-396 (2012).
24. Y. Han *et al.*, *Proceedings of the National Academy of Sciences* **117**, 5184 (2020).
25. P. U. Clark, J. D. Shakun, Y. Rosenthal, P. Köhler, P. J. Bartlein, *Science* **383**, 884-890 (2024).
- 25 26. R. Bintanja, R. S. W. van de Wal, *Nature* **454**, 869 (2008).
27. K. A. Jakob *et al.*, *Proceedings of the National Academy of Sciences* **117**, 30980-30987 (2020).
28. J. Sutter *et al.*, *The Cryosphere* **13**, 2023-2041 (2019).
29. Y. Yan *et al.*, *Nature* **574**, 663-666 (2019).
- 30 30. A. Martínez-García, A. Rosell-Melé, E. L. McClymont, R. Gersonde, G. H. Haug, *Science* **328**, 1550-1553 (2010).
31. E. W. Wolff *et al.*, *Nature* **440**, 491-496 (2006).
32. G. Knorr, G. Lohmann, *Nature Geoscience* **7**, 376-381 (2014).
33. S.-I. Shin, Z. Liu, B. L. Otto-Bliesner, J. E. Kutzbach, S. J. Vavrus, *Geophysical Research Letters* **30**, 1096 (2003).
- 35 34. D. M. Sigman, E. A. Boyle, *Nature* **407**, 859-869 (2000).
35. D. M. Sigman, S. L. Jaccard, G. H. Haug, *Nature* **428**, 59-63 (2004).
36. X. Zhang, G. Lohmann, G. Knorr, X. Xu, *Climate of the Past* **9**, 2319-2333 (2013).
37. E. Galbraith, C. de Lavergne, *Clim. Dyn.* **52**, 653-679 (2019).
- 40 38. C. Stepanek, E. Samakinwa, G. Knorr, G. Lohmann, *Climate of the Past* **16**, 2275-2323 (2020).
39. J. C. H. Chiang, C. M. Bitz, *Clim. Dyn.* **25**, 477-496 (2005).
40. J. R. Toggweiler, J. L. Russell, S. R. Carson, *Paleoceanography* **21**, PA2005 (2006).
41. R. McKay *et al.*, *Proceedings of the National Academy of Sciences* **109**, 6423 (2012).
- 45 42. T. Struve *et al.*, *Nature Communications* **11**, 5655 (2020).
43. Z. An *et al.*, *Science* **333**, 719-723 (2011).
44. R. S. Lindzen, B. Farrell, *Journal of Atmospheric Sciences* **37**, 1648-1654 (1980).
45. L. C. Peterson *et al.*, *Paleoceanography and Paleoclimatology* **35**, e2019PA003720 (2020).

46. E. L. McClymont *et al.*, *Paleoceanography* **31**, 895-913 (2016).
47. K. Pahnke, J. P. Sachs, *Paleoceanography* **21**, PA2003 (2006).
48. K. T. Lawrence, S. Sosdian, H. E. White, Y. Rosenthal, *Earth and Planetary Science Letters* **300**, 329-342 (2010).
- 5 49. B. D. A. Naafs, J. Hefter, R. Stein, *Quaternary Science Reviews* **80**, 1-28 (2013).
50. K. T. Lawrence, T. D. Herbert, C. M. Brown, M. E. Raymo, A. M. Haywood, *Paleoceanography* **24**, PA2218 (2009).
51. Z. Liu, L. C. Cleaveland, T. D. Herbert, *Earth and Planetary Science Letters* **265**, 703-715 (2008).
- 10 52. M. C. A. Catunda *et al.*, *Geophysical Research Letters* **48**, e2020GL091899 (2021).
53. S. A. Marcott, J. D. Shakun, P. U. Clark, A. C. Mix, *Science* **339**, 1198-1201 (2013).
54. C. L. Batchelor *et al.*, *Nature Communications* **10**, 3713 (2019).
55. E. J. Rohling *et al.*, *Nature Communications* **10**, 5040 (2019).
56. E. J. Gowan *et al.*, *Nature Communications* **12**, 1199 (2021).
- 15 57. T. Pico, J. R. Creveling, J. X. Mitrovica, *Nature Communications* **8**, 15612 (2017).
58. R. M. Spratt, L. E. Lisiecki, *Climate of the Past* **12**, 1079-1092 (2016).
59. K. Lambeck, H. Rouby, A. Purcell, Y. Sun, M. Sambridge, *Proceedings of the National Academy of Sciences* **111**, 15296-15303 (2014).
60. S. Barker *et al.*, *Paleoceanography and Paleoclimatology* **36**, e2020PA004200 (2021).
- 20 61. E. Roeckner *et al.*, (2003).
62. V. Brovkin, T. Raddatz, C. H. Reick, M. Claussen, V. Gayler, *Geophysical research letters* **36**, L07405 (2009).
63. S. J. Marsland, H. Haak, J. H. Jungclauss, M. Latif, F. Röske, *Ocean modelling* **5**, 91-127 (2003).
- 25 64. W. D. Hibler, *Journal of physical oceanography* **9**, 815-846 (1979).
65. W. Wei, G. Lohmann, *Journal of Climate* **25**, 6989-7002 (2012).
66. X. Gong, G. Knorr, G. Lohmann, X. Zhang, *Geophysical Research Letters* **40**, 3698-3704 (2013).
67. M. Stürz, W. Jokat, G. Knorr, G. Lohmann, *Nature communications* **8**, 1-13 (2017).
- 30 68. X. Zhang, G. Lohmann, G. Knorr, C. Purcell, *Nature* **512**, 290-294 (2014).
69. X. Zhang, G. Knorr, G. Lohmann, S. Barker, *Nature Geoscience* **10**, 518-523 (2017).
70. H. Dowsett *et al.*, *Climate of the Past* **12**, 1519-1538 (2016).
71. Z. Zhang, G. Li, H. Yan, Z. An, *Quaternary International* **464**, 364-369 (2018).
72. Y. Sun, S. C. Clemens, Z. An, Z. Yu, *Quaternary Science Reviews* **25**, 33-48 (2006).
- 35 73. B. de Boer, L. J. Lourens, R. S. W. van de Wal, *Nature Communications* **5**, 2999 (2014).
74. A. S. Hein *et al.*, *Nature Communications* **7**, 10325 (2016).
75. D. Fink, B. McKelvey, M. J. Hambrey, D. Fabel, R. Brown, *Earth and Planetary Science Letters* **243**, 229-243 (2006).
76. M. Yamane *et al.*, *Nature Communications* **6**, 7016 (2015).
- 40 77. K. Joy, D. Fink, B. Storey, C. Atkins, *Quaternary Science Reviews* **83**, 46-57 (2014).
78. K. M. Swanger, D. R. Marchant, J. M. Schaefer, G. Winckler, J. W. Head, *Global and Planetary Change* **79**, 61-72 (2011).
79. S. Strasky *et al.*, *Antarctic Science* **21**, 59-69 (2009).
80. T. Liu, *Loess and the Environment*. (China Ocean Press Beijing, 1985).
- 45 81. J. Xiao, Z. An, *Palaeogeography, Palaeoclimatology, Palaeoecology* **154**, 179-189 (1999).
82. G. Kukla, Z. An, *Palaeogeography, Palaeoclimatology, Palaeoecology* **72**, 203-225 (1989).
83. Z. Ding, Z. Yu, N. W. Rutter, T. Liu, *Quaternary Science Reviews* **13**, 39-70 (1994).

84. S. C. Porter, Z. An, *Nature* **375**, 305-308 (1995).
85. Z. S. An *et al.*, *Science in China Series B* **11**, 1209-1215 (1991).
86. G. Bartoli, B. Hönisch, R. E. Zeebe, *Paleoceanography* **26**, PA4213 (2011).
87. T. B. Chalk *et al.*, *Proceedings of the National Academy of Sciences* **114**, 13114 (2017).
- 5 88. B. Hönisch, N. G. Hemming, D. Archer, M. Siddall, J. F. McManus, *Science* **324**, 1551-1554 (2009).
89. M. A. Martínez-Botí *et al.*, *Nature* **518**, 49 (2015).
90. O. Seki *et al.*, *Earth and Planetary Science Letters* **292**, 201-211 (2010).
91. K. A. Dyez, B. Hönisch, G. A. Schmidt, *Paleoceanography and Paleoclimatology* **33**, 1270-1291 (2018).
- 10 92. G. L. Foster, *Earth and Planetary Science Letters* **271**, 254-266 (2008).
93. M. J. Henehan *et al.*, *Earth and Planetary Science Letters* **364**, 111-122 (2013).
94. P. N. Pearson, M. R. Palmer, *Nature* **406**, 695-699 (2000).
95. J. W. B. Rae *et al.*, *Annual Review of Earth and Planetary Sciences*, (2021).
- 15 96. S. M. Sosdian *et al.*, *Earth and Planetary Science Letters* **498**, 362-376 (2018).
97. L. B. Stap *et al.*, *Earth and Planetary Science Letters* **439**, 1-10 (2016).
98. B. Hönisch, N. G. Hemming, *Earth and Planetary Science Letters* **236**, 305-314 (2005).
99. J.-R. Petit *et al.*, *Nature* **399**, 429-436 (1999).
100. S. Urs *et al.*, *Science* **310**, 1313-1317 (2005).
- 20 101. L. Dieter *et al.*, *Nature* **453**, 379-382 (2008).
102. J. A. Higgins *et al.*, *Proceedings of the National Academy of Sciences* **112**, 6887-6891 (2015).
103. Z. Zhang, G. Li, Y. Cai, Z. Liu, Z. An, *Journal of Quaternary Science* **36**, 1214-1220 (2021).
- 25 104. Z. Zhang *et al.*, *Geophysical Research Letters* **49**, e2021GL096773 (2022).
105. X. Meng *et al.*, *Earth and Planetary Science Letters* **486**, 61-69 (2018).
106. W. Balsam, J. Ji, J. Chen, *Earth and Planetary Science Letters* **223**, 335-348 (2004).
107. J. Ji *et al.*, *Quaternary Sciences* **27**, (2007).
108. P. D. Clift *et al.*, *Nature Geoscience* **1**, 875 (2008).
- 30 109. Y. Sun *et al.*, *Nature Communications* **10**, 352 (2019).
110. R. A. Locarnini *et al.*, in *World Ocean Atlas 2013*, S. Levitus, A. Mishonov, Eds. (NOAA Atlas NESDIS, 2013), vol. 73, pp. 40.
111. E. A. Cowan, C.-D. Hillenbrand, L. E. Hassler, M. T. Ake, *Palaeogeography, Palaeoclimatology, Palaeoecology* **265**, 275-291 (2008).
- 35 112. S. Becquey, R. Gersonde, *Palaeogeography, Palaeoclimatology, Palaeoecology* **182**, 221-239 (2002).
113. M. E. Weber *et al.*, *Nature Communications* **13**, 2044 (2022).
114. L. D. Pena, S. L. Goldstein, *Science* **345**, 318-322 (2014).
115. R. Hu *et al.*, *Earth and Planetary Science Letters* **455**, 106-114 (2016).
- 40 116. C. Teschner, M. Frank, B. A. Haley, J. Knies, *Paleoceanography* **31**, 582-599 (2016).
117. V. Dausmann, M. Frank, M. Gutjahr, J. Rickli, *Paleoceanography* **32**, 265-283 (2017).
118. S. Barker *et al.*, *Science* **376**, 961-967 (2022).
119. N. Harada, M. Sato, T. Sakamoto, *Paleoceanography* **23**, PA3201 (2008).
120. E. Calvo, J. Villanueva, J. O. Grimalt, A. Boelaert, L. Labeyrie, *Earth and Planetary Science Letters* **188**, 509-519 (2001).
- 45 121. A. Cortina, F. J. Sierro, J. A. Flores, B. Martrat, J. O. Grimalt, *Geophysical Research Letters* **42**, 10,366-310,374 (2015).
122. J. Lattaud *et al.*, *Paleoceanography and Paleoclimatology* **33**, 732-744 (2018).

123. I. Koizumi, H. Yamamoto, *Marine Micropaleontology* **74**, 108-118 (2010).
124. E. S. Kandiano, H. A. Bauch, *Terra Nova* **15**, 265-271 (2003).
125. S. L. Ho *et al.*, *Paleoceanography* **27**, PA4202 (2012).
126. K. Pahnke, R. Zahn, H. Elderfield, M. Schulz, *Science* **301**, 948-952 (2003).
5 127. D. Nürnberg, J. Groeneveld, *Geochemistry, Geophysics, Geosystems* **7**, Q04P11 (2006).
128. A. P. Hasenfratz *et al.*, *Science* **363**, 1080 (2019).
129. G. Cortese, A. Abelmann, R. Gersonde, *Paleoceanography* **22**, PA4203 (2007).
130. S. Becquey, R. Gersonde, *Paleoceanography* **18**, 1014 (2003).
131. G. Schaefer *et al.*, *Marine Micropaleontology* **54**, 191-212 (2005).
10 132. B. W. Hayward *et al.*, *Global and Planetary Change* **63**, 309-316 (2008).
133. W. R. Howard, W. L. Prell, *Paleoceanography* **7**, 79-117 (1992).
134. L. Labeyrie *et al.*, *Paleoceanography* **11**, 57-76 (1996).
135. J.-J. Pichon *et al.*, *Paleoceanography* **7**, 289-318 (1992).
15 136. IPCC, *Climate Change 2007: Synthesis Report. Contribution of Working Groups I, II and III to the Fourth Assessment Report of the Intergovernmental Panel on Climate Change.* (Geneva, Switzerland, 2007).

Acknowledgments: The research was supported by Chinese Academy of Sciences (including XDB40000000 and others), the Basic Science Center for Tibetan Plateau Earth System (BSCTPES, NSFC project No. 41988101), the Fund of Shandong Province (No. LSKJ202203300), National Natural Science Foundation of China, and Chinese Ministry of Science and Technology. Gerrit Lohmann and Christian Stepanek acknowledge institutional funding from the Alfred Wegener Institute (AWI) via the research programme PACES-II of the Helmholtz Association. Christian Stepanek acknowledges funding from the Helmholtz Climate Initiative REKLIM. Climate modeling was performed on Tianhe new generation supercomputer at National Supercomputer Center in Tianjin. In particular, An Zhisheng acknowledges the selfless support from Yihe Tai.

Author contributions: A.Z.S., W.J.Z., Z.K.Z., Z.H.L., X.Z. and Y.B.S. designed and conducted the research. X.Z. led the climate modelling and analysis. J.J.Z., A.Z.S., Z.H.L., Y.B.S., J.M.Y., X.L.M., Y.J.C., H.Y., X.Z., W.J.Z. and Z.K.Z. conducted reconstruction of hemispheric ice sheets and analysis. Z.K.Z., G.J.L. and T.L. generated the Pleistocene Asian monsoon record. A.Z.S., Z.H.L., X.Z., Y.B.S., S.C.C., Z.K.Z., Z.G.S., X.L.M., J.J.Z., W.J.Z., Y.J.C. and G.C.D. wrote the paper and analyzed the data. X.Z. designed and conducted model experiments with aid of Y.S., C.S. and G.L.. Y.C.S, S.Q.L. and Y.A.Z. postprocessed model outputs under supervision of X.Z. and Z.G.S.. T.L. and Y.F.H. collected samples and data. L.X.W., W.J.C., H.C., Y.J.C., Y.L., Z.D.J., C.S., J.M.Y. and J.L. provided feedback on the analyses, the figures and the manuscript. All authors contributed to the preparation of the manuscript.

Competing interests: Authors declare that they have no competing interests.

Data and materials availability: All relevant proxy records that support the findings of this research are available at the East Asian Paleoenvironmental Science Database

(http://paleodata.ieecas.cn/FrmDataInfo_EN.aspx?id=9e546f03-8e66-4d73-878e-a9639488ce0b).

Supplementary Materials

5

Materials and Methods

Supplementary Text

Figs. S1 to S14

Tables S1 to S3

References (45-136)

10

Figure legends

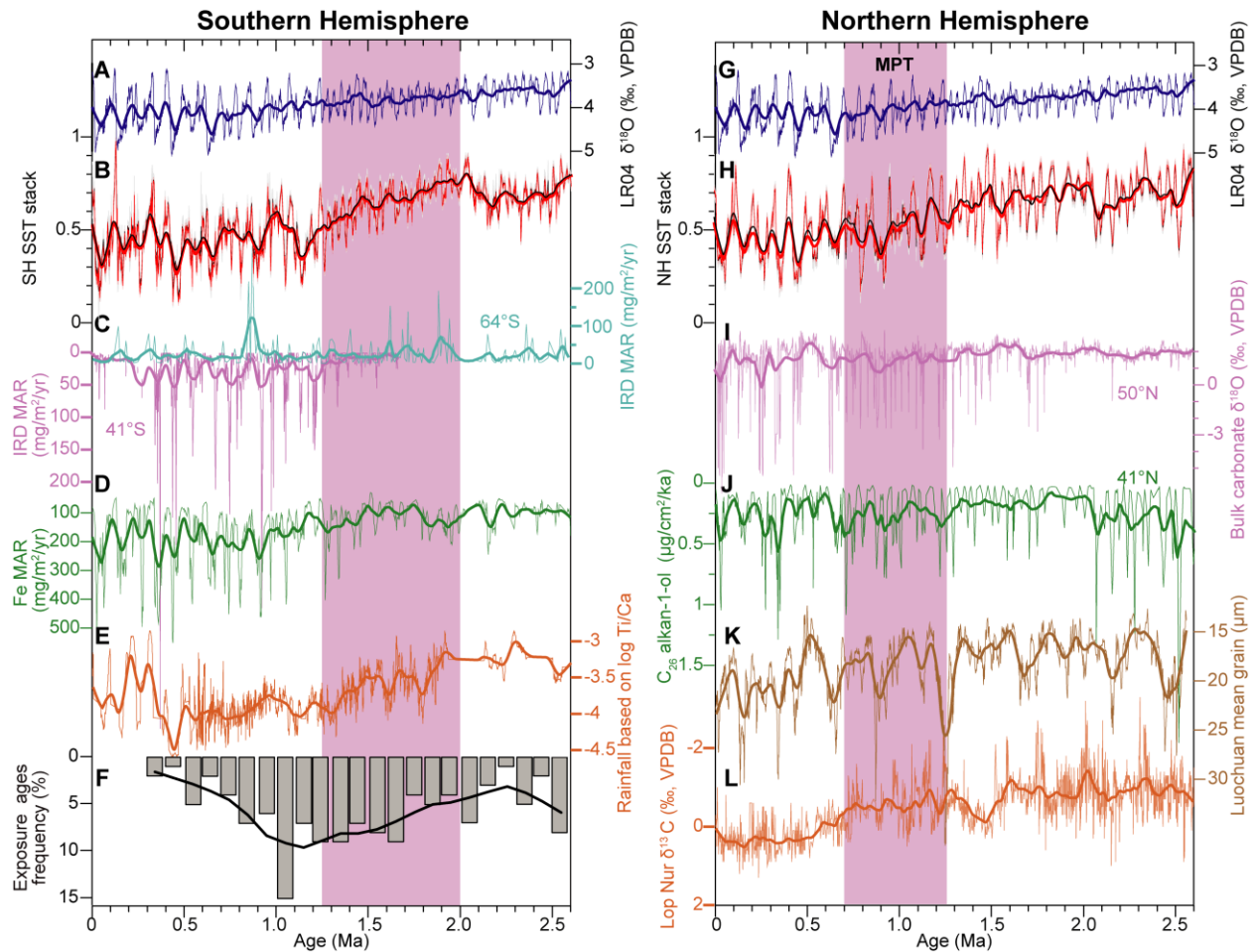


Fig. 1. Geological evidence for asynchronous development of hemispheric ice sheets. (A, G) Global $\delta^{18}\text{O}$ stack (2). (B, H) Southern Hemisphere (SH) and Northern Hemisphere (NH) mid-latitude SST stacks with consideration of ± 0.5 kyr age error. (C) Ice rafted debris (IRD) records from Agulhas Plateau (AP) and ODP 1101 (11, 14), inferred increased Antarctic Ice Sheet (AIS) and sea ice plotted downward. (D) Fe mass accumulation rate (MAR) from ODP 1090 (15). (E) Ti/Ca record off Australia (16). (F) Histogram of exposure ages at Roberts Massif (17). (I) Bulk carbonate $\delta^{18}\text{O}$ record from IODP U1308 (18). (J) Dust record from IODP 1313 (19). (K) Loess grain size at Luochuan (23). (L) Carbonate $\delta^{13}\text{C}$ at Lop Nur (20). Thick lines show 100-kyr running averages (600-kyr average in F). Purple shading indicates the period of rapid ice sheet growth in each hemisphere. Gray shadings show the SST stack uncertainty (2σ) in B and H. More extensive IRD and dust records from the Southern Ocean and the North Atlantic Ocean shown in fig. S3 and fig. S4 respectively. Site location information in fig. S1.

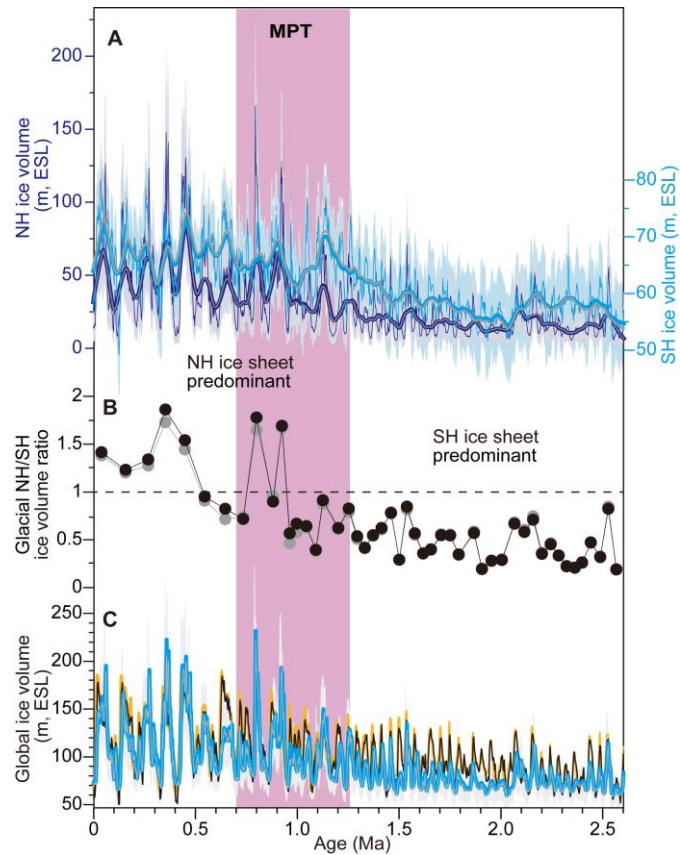


Fig. 2. SST-derived Pleistocene hemispheric ice-sheet development. (A) Southern Hemisphere (SH) (light blue) and Northern Hemisphere (NH) (dark blue) ice-sheet development (in units of ESL). (B) The ratios of NH and SH glacial ice volume. (C) Reconstructed global ice volume as inferred from SST stacks (blue), the global benthic $\delta^{18}\text{O}$ stack (2) (black), and model simulations (24) (yellow). Our estimate of hemispheric and global ice volume with an age error of ± 0.5 kyr in SST records is presented here (estimates with other age errors in fig. S9). Thick lines in A denote 100-kyr running averages. Shadings in A and C denote uncertainty (1σ).

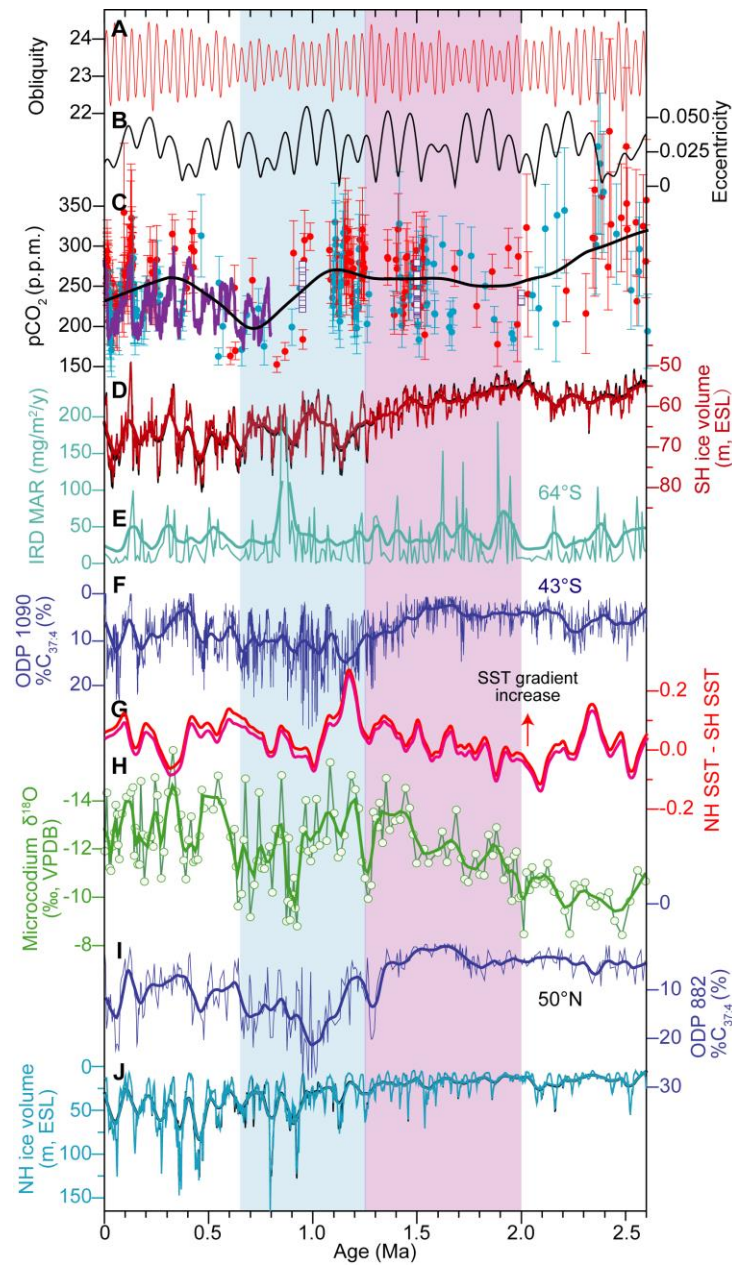


Fig. 3. Asynchronous development of hemispheric ice sheets/sea ice triggering the MPT. (A) Obliquity. (B) Eccentricity. (C) Atmospheric CO₂ (red dots: interglacials; blue dots: glacials; purple lines and open squares: ice core CO₂, Supplementary Text). (D) Reconstructed Southern Hemisphere (SH) ice volume; (E, F) Southern Ocean ice rafted debris (IRD) (E) and %C_{37:4} (sea-ice proxy) (F) records. (G) Difference between the Northern Hemisphere (NH) and SH SST stacks after 100-kyr smoothing. (H) Loess microcodium $\delta^{18}\text{O}$ record. (I) North Pacific %C_{37:4} record (26). (J) Reconstructed NH ice volume. Grey shadings denote uncertainty (1 σ) in D and J. Thick lines are 100-kyr running average in D-J (600-kyr average in C). Purple and blue shadings indicate periods of substantial ice-sheet growth in the SH and NH, respectively.

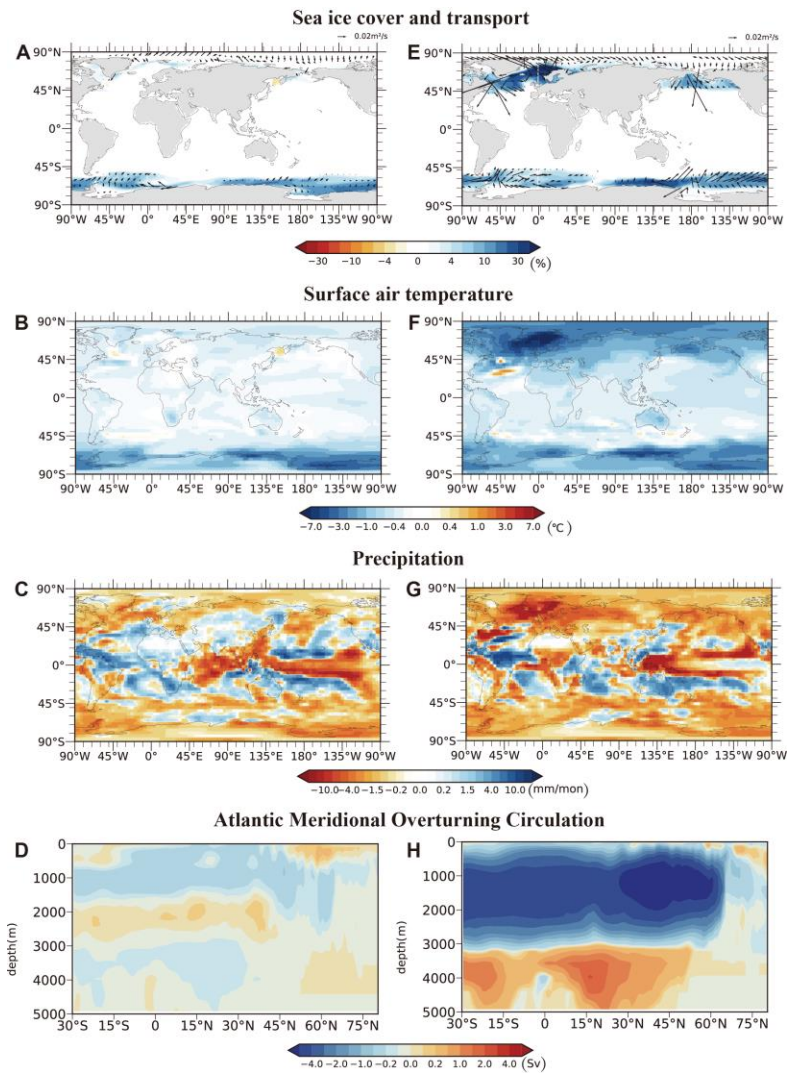


Fig. 4 | Global climatic responses to Antarctic Ice Sheet expansion under interglacial and glacial CO₂ levels. (A) Annual mean sea ice cover (shading; %) and transport (vector; m²/s), (B) surface air temperature (°C), (C) precipitation (mm/month) and (D) Atlantic meridional overturning circulation (AMOC, Sv), all under interglacial CO₂ level (280 ppm). E, F, G and H are the same as A, B, C, and D, respectively, but under glacial CO₂ level (220 ppm).

5